



Cite this: *New J. Chem.*, 2023, 47, 17174

## An amine-rich porous organic polymer with flexible diarylmethane moieties for adsorptive removal of anionic dyes

Atena Rashidinia and Mohammad Dinari  \*

Developing porous organic polymers (POPs) as efficient adsorbents for wastewater treatment began a new era in environmental remediation. In the current paper, an amine-rich triazine-based POP with excellent flexibility, denoted as MDA-POP, was synthesized using a facile method from accessible building blocks. The prepared MDA-POP was thoroughly characterized using various analytical techniques and its application in removing Congo red and Scarlet 4BS, two widely used textile colors, was investigated. The optimal conditions for the adsorption process were determined by studying different effective parameters, including pH, temperature, adsorbent dosage, and contact time. By optimizing the adsorption conditions, the dye removal efficiency reached up to 99%, with maximum adsorption capacities of  $71.43 \text{ mg g}^{-1}$  for Congo red and  $136.97 \text{ mg g}^{-1}$  for Scarlet 4BS. The adsorption isotherms of both the dyes were best fitted to the Langmuir model, which indicates monolayer adsorption. Moreover, the study on the kinetic aspects of adsorption shows that the pseudo-second-order model is the best model for describing the adsorption process; thus, the chemical interactions play a vital role in the rate-determining step of the adsorption. The thermodynamic studies show that the standard enthalpies of adsorption ( $\Delta H^\circ$ ) are  $-178.8 \text{ kJ mol}^{-1}$  for Congo red and  $-75.4 \text{ kJ mol}^{-1}$  for Scarlet 4BS, indicating that the nature of adsorption is chemisorption. Also, the negative standard free Gibb's energy ( $\Delta G^\circ$ ) values reveal a spontaneous adsorption process. This paper provides a facile and efficient method for synthesizing POPs as adsorbents for water treatment applications.

Received 27th April 2023,  
Accepted 24th July 2023

DOI: 10.1039/d3nj01950k

rsc.li/njc

### 1. Introduction

Due to the growth of the human population and the discharge of organic pollutants into the environment, much effort has been devoted to treat industrial wastes. Organic dyes are the most frequently seen pollutants in wastewater released from food and plastic, paper printing, cosmetic, and textile dyeing industries.<sup>1</sup> Also, they may cause severe damage to microorganisms, human health, and aquatic ecosystems.<sup>2</sup> Several effective strategies have been developed to remove toxic organic dyes from water and wastewater sources. Coagulation,<sup>3</sup> photocatalysis,<sup>4–6</sup> and oxidative degradation<sup>7</sup> are the most used methods for removing dyes. Compared to these methods, adsorption gained paramount interest because of its easy manipulation and cost-effectiveness for the direct adsorption of organic contaminants from water resources.<sup>8,9</sup>

Several types of compounds have been reported to be used as adsorbents, including mesoporous silicas,<sup>10</sup>

metal–organic frameworks (MOFs),<sup>11,12</sup> zeolites,<sup>13,14</sup> activated carbonaceous materials,<sup>15–18</sup> and porous organic polymers (POPs).<sup>19–21</sup> Among them, activated carbon and other carbonaceous materials suffer from a small pore size, MOFs suffer from instability in acidic solutions, and zeolites and mesoporous silicas suffer from hard functionalization leading to limited application in dye removal.<sup>22</sup> Therefore, finding cost-effective materials with rapid, efficient, and selective adsorption of toxic organic dyes has become a long-lasting challenge.<sup>23</sup> POPs are a relatively young class of porous materials with excellent and unique properties, including ease of functionalization, adjustable porosity, and structural diversity.<sup>23,24</sup>

POPs' properties made them have potential applications in optoelectronics,<sup>25,26</sup> gas storage and separation,<sup>27–32</sup> adsorption,<sup>33–35</sup> and catalysis.<sup>36–39</sup> More importantly, the adsorption properties of POPs can be easily improved by post-synthetic modifications, heteroatom-containing building blocks, and generating constricted pores.<sup>40</sup>

In this paper, we report an amine-rich porous organic polymer (MDA-POP) synthesised using a polymerization reaction between 4,4'-methyleneedianiline (MDA) and 2,4,6-trichloro-1,3,5-triazine (TCT) and use it as an adsorbent for

Department of Chemistry, Isfahan University of Technology, Isfahan 84156-83111, Iran. E-mail: dinari@iut.ac.ir, mdinari@gmail.com; Fax: +98-31-3391-2350; Tel: +98-31-3391-3270

removing anionic dyes from aqueous solutions. Congo red and Scarlet 4BS were selected as the objective removal models to understand the prepared MDA-POP's adsorption abilities. The batch adsorption experiments were conducted systematically to investigate the effects of parameters such as adsorbent dosage, solution pH, adsorption time, and temperature on the adsorption. Also, the obtained MDA-POP shows excellent reusability for three successive cycles.

## 2. Experimental

### 2.1. Reagents and materials

2,4,6-Trichloro-1,3,5-triazine (TCT), 4,4'-methylenedianiline (MDA), sodium hydroxide, 1,4-dioxane, acetic acid, acetone, and hydrochloric acid (37%) were purchased from Merck Chemical Company (Germany). All the other chemicals were used without further purification.

### 2.2. Instrumentation

A Rigaku Rint 2000 diffractometer (Japan) with a Cu K $\alpha$  source (1.5406 Å) was used under the operating conditions of 40 kV and 40 mA to record the X-ray diffraction (XRD) pattern. An Autosorb-iQ (Quantachrome, USA) was used to analyze the N<sub>2</sub> adsorption/desorption isotherms at 77 K. The Brunauer–Emmett–Teller (BET) method was employed to estimate the specific surface area of MDA-POP. A Hitachi S-4800 at an accelerating voltage of 5 kV was utilized to study the surface morphology of the samples. A Thermo Scientific Nicolet 4700 spectrometer was also used to record FTIR spectra to investigate the functional groups. Moreover, a Hitachi HT-Seiko Exter 6300 was used to determine the thermal stability. The heating rate under the nitrogen flow was 10 °C min<sup>-1</sup>.

### 2.3. Synthesis of MDA-POP

MDA-POP was prepared using a modified procedure presented elsewhere.<sup>41</sup> Typically, a 100 mL round-bottom flask was filled with MDA (590 mg, 3 mmol) and NaOH (240 mg, 6 mmol) in 30 mL 1,4-dioxane and let it stir for 20 min. In a separate container, TCT (369 mg, 2 mmol) was dissolved in 30 mL 1,4-dioxane. Then, it was added to the previous solution in a dropwise manner. The obtained mixture was refluxed under a N<sub>2</sub> atmosphere for 24 h. After reaction completion, the light yellowish precipitated product was filtrated and washed with 1,4-dioxane to remove the unreacted starting materials and oligomers. Then, it was dried at 75 °C for 12 h.

### 2.4. Dye adsorption studies

Congo red and Scarlet 4BS (marked as Scarlet for briefing) were used as model anionic dyes for adsorption studies. The adsorption isotherms were investigated using different isotherm models, including Langmuir, Freundlich, Dubinin–Radushkevich, and Temkin models. Moreover, the kinetics of the adsorption

was investigated using pseudo-first-order, pseudo-second-order Elovich, and intraparticle diffusion (IPD) kinetic models. Also, the effect of temperature on the adsorption was evaluated using the van't Hoff equation.

**2.4.1. Adsorption isotherm.** The adsorption isotherm was established by varying the dye's initial concentration ( $C_i$ ) from 100 to 300 mg L<sup>-1</sup>. For each experiment, a screw-capped vial was filled with 5 mL of dye solution and 6 mg of the adsorbent. The mixture was stirred until the concentration was equilibrated. Then, the concentration at equilibrium ( $C_e$ ) was obtained using the UV-Vis spectra. The obtained data were fitted to different isotherm models.<sup>42</sup> The Langmuir isotherm is shown in eqn (1):

$$\frac{C_e}{q_e} = \frac{1}{K_L q_{\max}} + \frac{C_e}{q_{\max}} \quad (1)$$

In this equation,  $q_{\max}$  (mg g<sup>-1</sup>) is the maximum adsorption capacity, and  $K_L$  (L mg<sup>-1</sup>) is the Langmuir constant.

The Freundlich isotherm is explained as eqn (2):

$$\log(q_e) = \log(K_F) + \frac{1}{n} \log(C_e) \quad (2)$$

where  $K_F$  is the Freundlich constant,  $n$  is the sorption intensity, and  $C_e$  (mg L<sup>-1</sup>) is the dye concentration at equilibrium.

The Dubinin–Radushkevich (eqn (3)) isotherm is expressed as the following logarithmic equation:

$$\ln q_e = \ln q_{DR} - B_{DR}\varepsilon^2 \quad (3)$$

where  $B_{DR}$  is the Dubinin–Radushkevich constant,  $q_{DR}$  (mg g<sup>-1</sup>) is the theoretical adsorption capacity, and  $\varepsilon$  is defined using the following equation:

$$\varepsilon = RT \ln\left(1 + \frac{1}{C_e}\right) \quad (4)$$

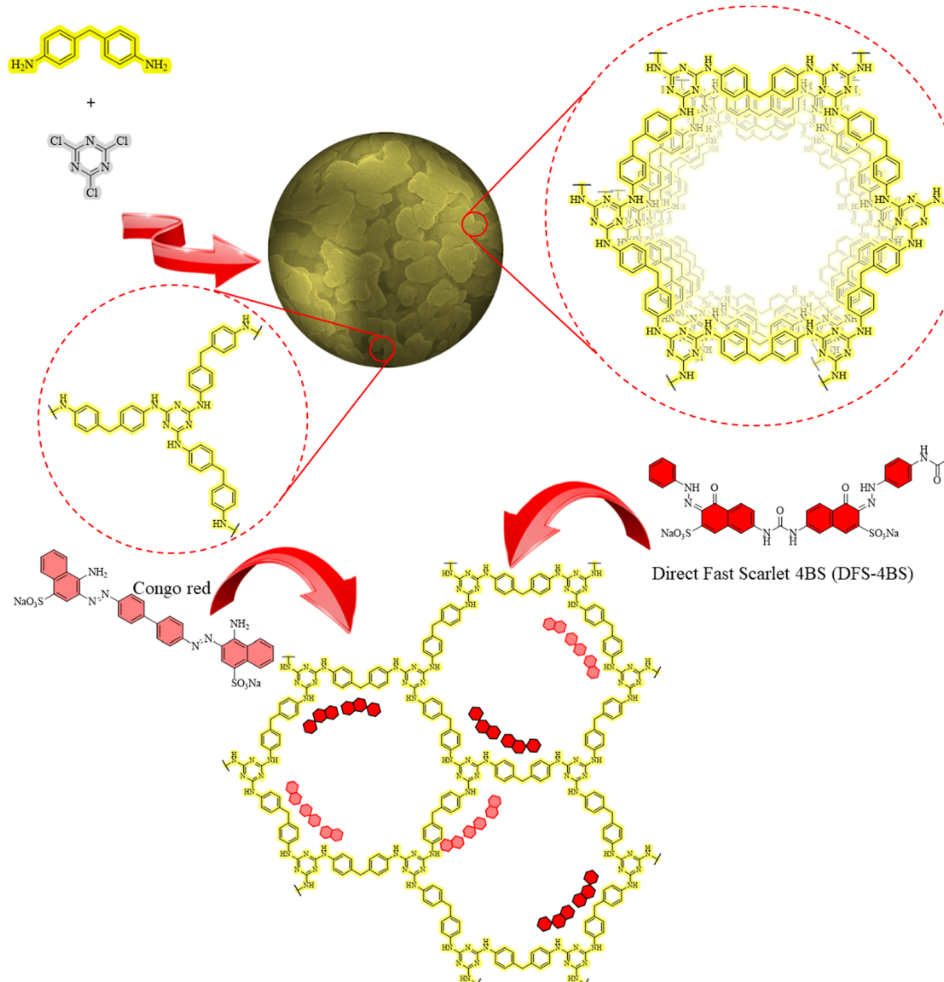
$R$  and  $T$  are the gas constant (8.314 J mol<sup>-1</sup> K<sup>-1</sup>) and the absolute temperature (K), respectively.

The following equation (eqn (5)) expressed the Temkin isotherm:

$$q_e = B \ln(C_e) + B \ln A \quad (5)$$

Temkin constants ( $A$  and  $B$ ) describe the adsorbate and adsorbent interactions.  $A$  denotes the equilibrium binding constant (L mg<sup>-1</sup>), and  $B$  is the maximum binding energy. Also,  $B$  directly depends on the absolute temperature ( $B = RT/b_T$ ).  $b_T$  is the Temkin constant that indicates the adsorption energy (kJ mol<sup>-1</sup>).<sup>43</sup>

**2.4.2. Adsorption kinetics.** The optimization study conducted reveals the best pH for each dye to be adsorbed. A screw-capped vial was filled with 6 mg of MDA-POP and 5 mL of Scarlet solution (100 mg L<sup>-1</sup>, pH = 4). Another vial was filled with 6 mg of MDA-POP and 5 mL of Congo red solution (100 mg L<sup>-1</sup>, pH = 5). The mixtures were sonicated for 2 min and stirred at room temperature for sufficient time. At each time interval, the mixture was centrifuged and the supernatant was subjected to UV-Vis spectrophotometry to determine the



**Scheme 1** The schematic illustration of the MDA-POP synthesis and its application in removing dyes.

concentration of the dyes. Thus, the removal efficiency ( $R_e$ ) can be obtained from the following equation<sup>44</sup>:

$$\% R_e = \frac{C_0 - C_t}{C_0} \times 100 \quad (6)$$

where  $C_t$  (mg L<sup>-1</sup>) is the concentration at a time interval ( $t$ ) and  $C_0$  (mg L<sup>-1</sup>) is the initial concentration. The adsorption capacity ( $q$ ) can be determined using the equation presented below<sup>45</sup>:

$$q_t = (C_0 - C_t) \frac{V}{m} \quad (7)$$

In this equation,  $m$  is the adsorbent mass (g),  $V$  is the solution volume, and  $q_t$  (mg g<sup>-1</sup>) is the adsorption capacity at a time interval ( $t$ ).

The most frequently used kinetic models are the pseudo-first-order and pseudo-second-order models. These models can be expressed as the following equations<sup>1</sup>:

$$\ln(q_e - q_t) = \ln q_e - K_1 t \quad \text{pseudo-first-order} \quad (8)$$

$$\frac{t}{q_t} = \frac{1}{K_2 \cdot q_e^2} + \frac{t}{q_e} \quad \text{pseudo-second-order} \quad (9)$$

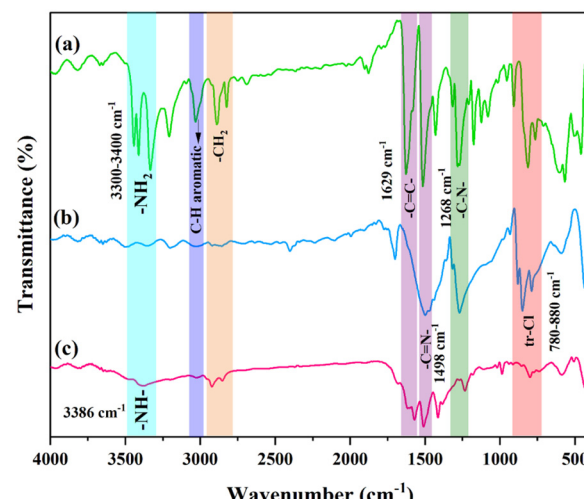


**Fig. 1** FTIR spectra of (a) MDA, (b) TCT, and (c) MDA-POP.

In these equations,  $K_1$  and  $K_2$  (g mg<sup>-1</sup> min<sup>-1</sup>) are the equilibrium rate constants of the pseudo-first-order and pseudo-second-order kinetic models, respectively.  $q_e$  (mg g<sup>-1</sup>)

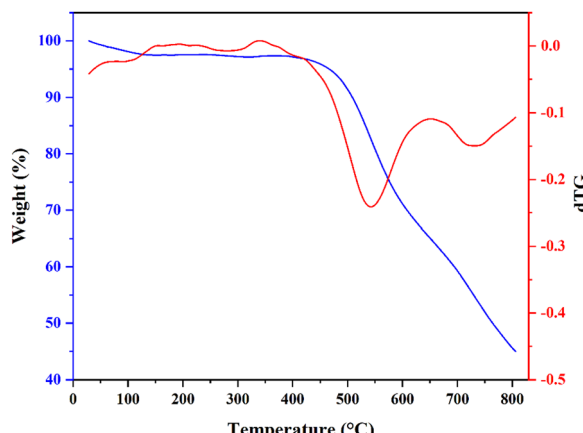


Fig. 2 TGA and dTG diagrams of MDA-POP.

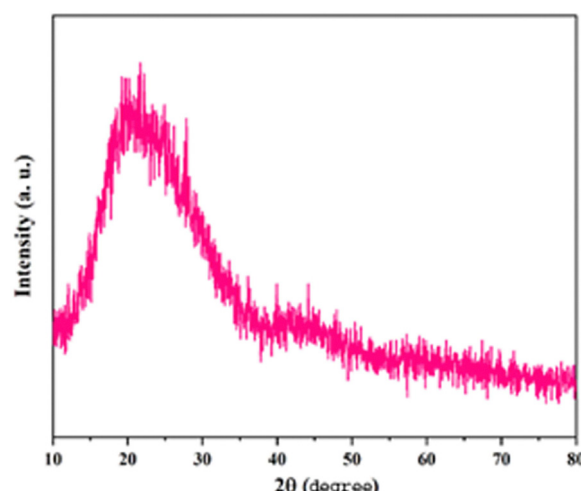


Fig. 3 XRD pattern of the MDA-POP.

and  $q_t$  ( $\text{mg g}^{-1}$ ) also stand for the amount of dye adsorbed per mass unit of the adsorbent at the equilibrium and the amount of dye adsorbed per mass unit of the adsorbent at time  $t$ , respectively.

The intraparticle diffusion (IPD) model was also used to investigate whether or not the diffusion is the rate-determining step of the adsorption. In this regard, the equation described by Weber and Morris<sup>46,47</sup> was used (eqn (10)):

$$q_t = K_{\text{id}} t^{1/2} + l \quad \text{IPD} \quad (10)$$

In this equation,  $l$  is the effect of boundary layer thickness and  $K_{\text{id}}$  is the IPD rate constant.

The Elovich model assumes that the adsorption and desorption cannot affect the adsorption rate. The Elovich model can be described using the following equation:

$$q_t = \frac{1}{\alpha} \ln(\alpha\beta) + \frac{1}{\alpha} \ln t \quad \text{Elovich} \quad (11)$$

In this equation,  $\alpha$  and  $\beta$  are the initial adsorption rate ( $\text{g mg}^{-1} \text{ min}^{-1}$ ) and the desorption constant ( $\text{mg g}^{-1} \text{ min}^{-1}$ ), respectively.

**2.4.3. Thermodynamic studies.** Sufficient information regarding the adsorption of Congo red and Scarlet as a function of temperature can be obtained from the Gibbs free energy changes using the classical van't Hoff equation (eqn (12)): <sup>48</sup>

$$\ln K_d = -\frac{\Delta H^\circ}{RT} + \frac{\Delta S^\circ}{R} \quad (12)$$

In this equation,  $\Delta G^\circ$  stands for the standard Gibbs free energy changes,  $\Delta H^\circ$  stands for the enthalpy changes, and  $\Delta S^\circ$  stands for the entropy changes. The sign of  $\Delta G^\circ$  is a measurement of the spontaneity of a process. Negative values for  $\Delta G^\circ$  represent a spontaneous adsorption process. Also,  $K_d$  is defined as the linear sorption distribution coefficient expressed as the following equation:

$$K_d = \frac{C_{ae}}{C_e} \quad (13)$$

In this equation,  $C_{ae}$  defines the quantity of the adsorbed dye per solution volume (L) at the equilibrium and  $C_e$  is the concentration at the equilibrium.<sup>49,50</sup>

**2.4.4. Recycling test.** To investigate the reusability, a series of consecutive cycles were conducted under the optimized conditions. After each experiment, the adsorbent was centrifuged and washed by soaking it in 20 mL of methanol, ethanol,

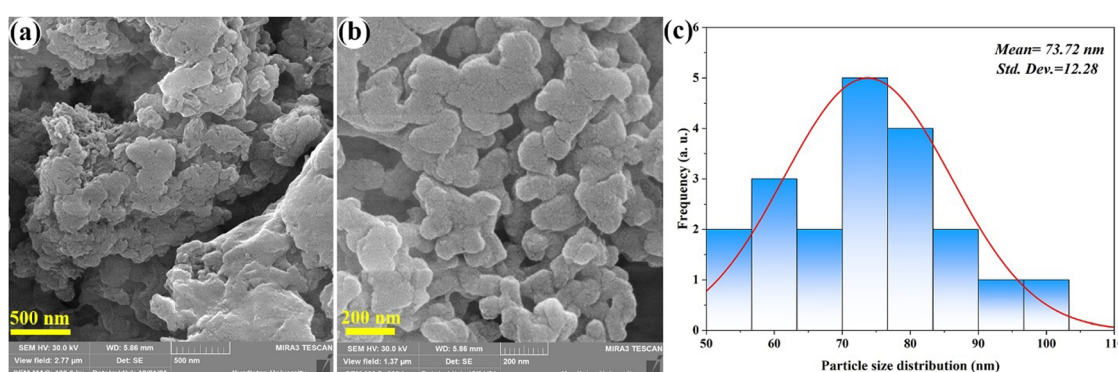


Fig. 4 (a) and (b) FESEM images of the MDA-POP and (c) its corresponding particle size distribution diagram.

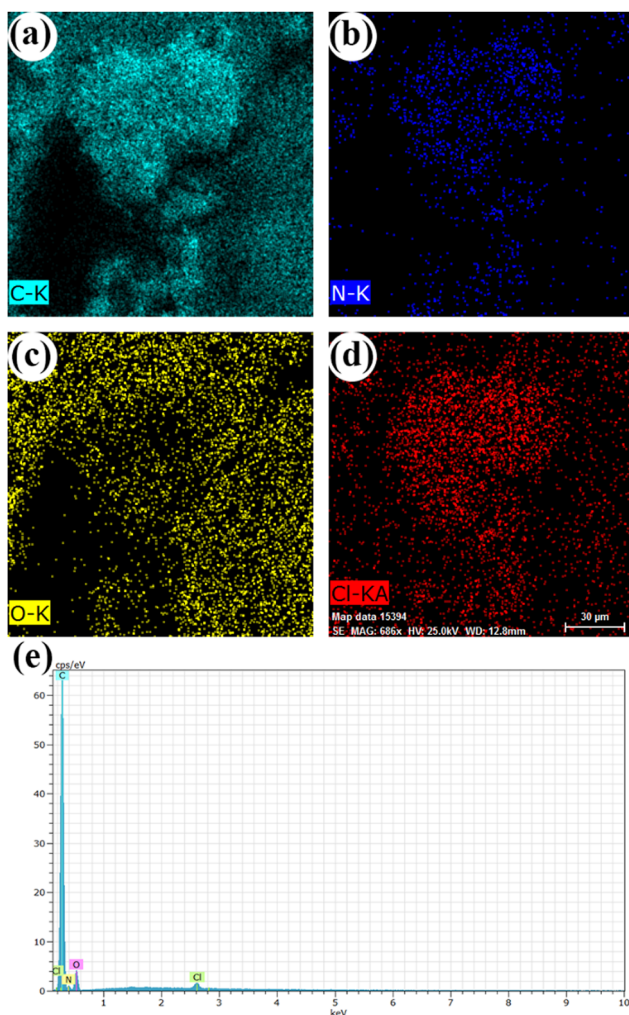


Fig. 5 (a)–(d) Elemental mapping images and (e) EDXA spectrum of the MDA-POP.

and acetone. Then, it was dried at 70 °C and used for the next cycle.

### 3. Results and discussion

MDA-POP was prepared by a polymerization reaction between MDA and TCT using NaOH in 1,4-dioxane to neutralize the released HCl during the reaction (Scheme 1). The reaction is completed by refluxing the mixture for 24 h. The pale-yellow precipitate was used as the adsorbent for removing anionic dyes from wastewater. The amine-rich nature of the adsorbent facilitates the formation of effective interactions between the adsorbate and adsorbent. Also, the presence of the  $-\text{CH}_2-$  group in the MDA can increase the degrees of freedom, enhancing the adsorption capability. Although MDA-POP shows excellent removal behavior for anionic dyes, the initial test for the adsorption of cationic dyes was unsatisfactory.

#### 3.1. Analytical characterization of MDA-POP

The functional group changes were studied using the FTIR analysis to confirm the formation of MDA-POP. As evidenced in Fig. 1, for the MDA structure, the  $-\text{NH}_2$  stretching vibrations were observed as two peaks at around 3300–3400  $\text{cm}^{-1}$  (Fig. 1a), which turned into a single peak at 3386  $\text{cm}^{-1}$  upon the reaction of MDA with TCT (Fig. 1c). Also, the bending vibration peaks of  $-\text{N}-\text{H}$  moieties were observed at 1610  $\text{cm}^{-1}$ . Moreover, the vibration peak of aromatic C-H bonds for the MDA-POP was observed at around 3050  $\text{cm}^{-1}$ . Similarly, the benzylic  $-\text{CH}_2-$  vibration peak was observed at around 2800–2900  $\text{cm}^{-1}$  for the MDA-POP in the FTIR spectra. The sharp peaks at around 1400–1600  $\text{cm}^{-1}$  correspond to the  $-\text{C}=\text{C}-$  and  $-\text{C}=\text{N}-$  vibrations in the aromatic and triazine rings, respectively. These results prove the successful formation of MDA-POP from the displacement reaction of MDA with chlorine in TCT.

The thermal stability of the prepared MDA-POP was analyzed using the TGA diagram. As shown in Fig. 2, the marginal weight loss that appeared at 134.5 °C is attributed to the release of solvents trapped inside the polymeric framework. Also, the presence of benzylic groups may cause a regular break of Ar- $\text{CH}_2$ -Ar at 522–800 °C. The  $T_{\text{d}5\%}$  and  $T_{\text{d}10\%}$  values of MDA-POP were found to be 466 °C and 508 °C, respectively. The char yield

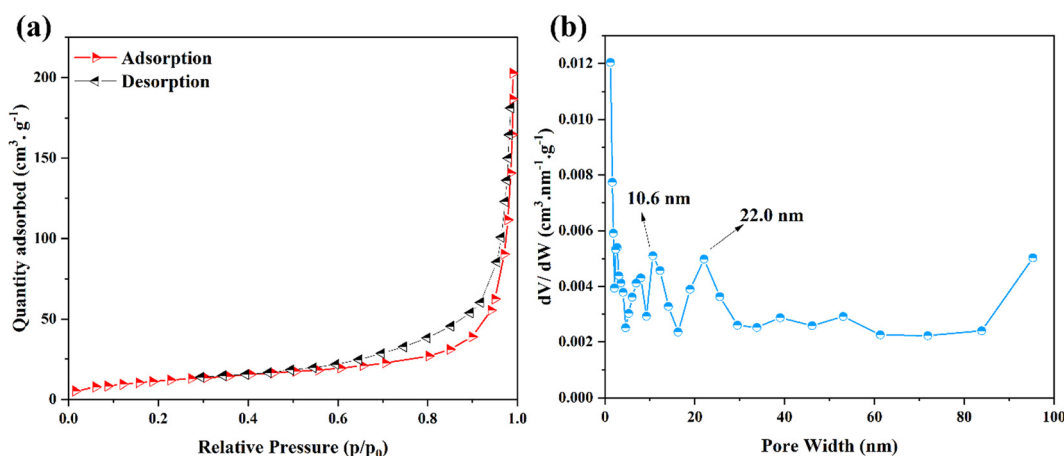


Fig. 6 (a)  $\text{N}_2$  adsorption/desorption diagram of MDA-POP and (b) the corresponding BJH diagram.

at 800 °C is found to be 45.6%. The presence of chlorine atoms in the MDA-POP structure can provide it the potential flame-retardant capability. The dTG curve also proved that the main decomposition appeared at 543 °C.

The crystallinity of the prepared MDA-POP was studied using the powder X-ray diffraction pattern analysis (Fig. 3). The MDA-POP shows two broad peaks centered at  $2\theta = 20^\circ$  and  $2\theta = 43^\circ$  representing an amorphous packing of the polymeric structure. This phenomenon is mainly due to the irreversibility of the displacement reaction during the MDA-POP formation.

The MDA-POP morphology was characterized using FESEM images. Fig. 4 represents the FESEM images of the MDA-POP, confirming its amorphous structure with a semi-spherical morphology. Importantly, the MDA-POP has a regular porous structure providing a facile route for adsorption of organic dyes. The particle size distribution shows a mean particle diameter of 74 nm. The elemental mapping and energy dispersive X-ray analysis (EDXA) shows a uniform distribution of elements over the surface of the MDA-POP (Fig. 5). This phenomenon implies that the displacement reaction occurs across the polymer chains providing a certain degree of structural regularity.

The specific surface area and porosity parameters of the MDA-POP were determined using the  $N_2$  adsorption/desorption isotherm, and the obtained results were fitted to the BET model (Fig. 6a). According to the IUPAC classification, the adsorption/desorption isotherm closely obeys the Type IV isotherm that is evidence of a mesoporous structure. Moreover, the hysteresis loop of the obtained isotherm is similar to the H3 type representing a non-rigid aggregate of plate-like particles. The specific surface area of the MDA-POP is found to be  $44 \text{ m}^2 \text{ g}^{-1}$ , and the mean pore width is estimated to be

1.2 nm (Fig. 6b). Also, the total pore volume of the sample is obtained to be  $0.31 \text{ cm}^3 \text{ g}^{-1}$ .

### 3.2. Adsorption properties

The results obtained from the analytical data and the presence of amine moieties in the MDA-POP structure reveal its potential for application in adsorbing organic water contaminants with hydrogen-bond and  $\pi-\pi$  stacking interactions. Considering that the study of the effects of parameters on the wastewater treatment is the first step to investigate any adsorption process, the effect of solution pH on the adsorption process cannot be

Table 1 The zeta potential values for the MDA-POP at different pHs

Compound	pH = 4	pH = 7	pH = 9
MDA-POP	$-2.73 \pm 0.76$	$-10.07 \pm 11$	$-4.33 \pm 2.24$

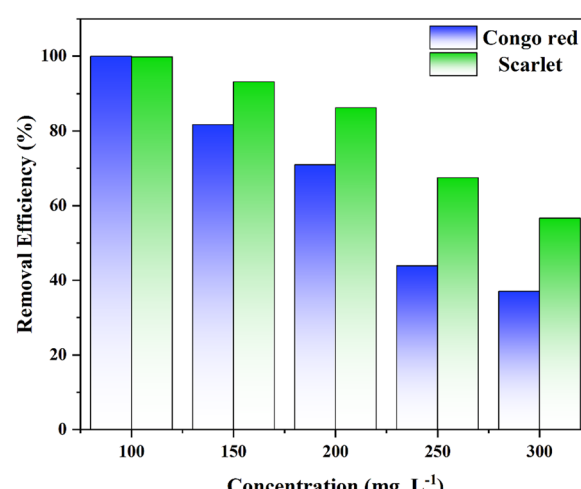


Fig. 8 The effect of the initial concentration of anionic dyes on the adsorption behavior of the MDA-POP under optimal conditions.

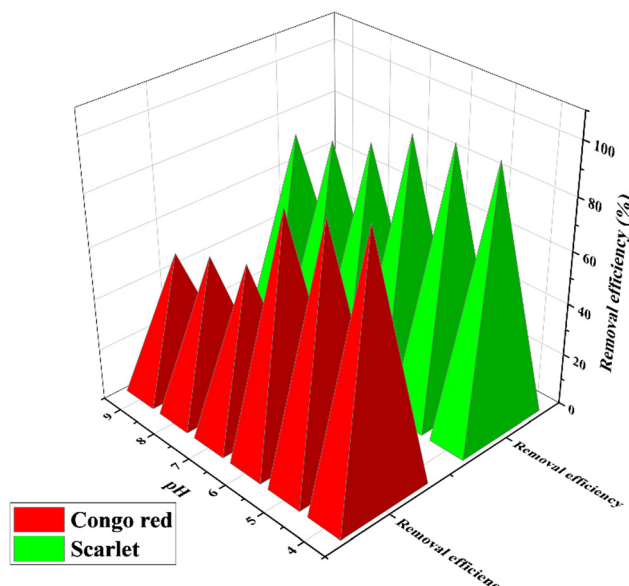


Fig. 7 The effect of pH values on the adsorption of anionic dyes under the optimal conditions.

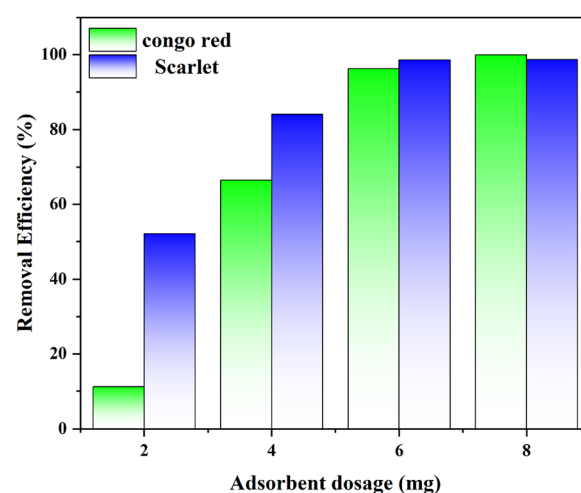


Fig. 9 Optimizing the amount of adsorbent dosage for the adsorption behavior.

ignored. Thus, the initial solution pH values were adjusted from 4–9 (Fig. 7) using standard NaOH or HCl solutions. Strong basic solutions were not explored due to the self-decomposition of dyes in a strong basic medium. As the pH values increased from 4 to 9, the removal efficiency ( $R_e$ ) gradually declined for both the model dyes. In the case of Congo red, the maximum  $R_e$  reached 94.5% at a pH value of 5.0, while  $R_e$  reached 99.5% at a pH value of 4.0 for Scarlet. The presence of hydrogen bonds and the  $\pi$ - $\pi$  stacking can synergistically increase the MDA-POP's removal efficiency. The presence of electrostatic interactions in

the adsorption process was investigated using the surface charge of the MDA-POP in three different pH values of 4, 7, and 9. Table 1 shows the zeta potential values for these three different pHs. As evidenced, the surface charge was negative in all three pHs, indicating that the electrostatic interactions were not responsible for the adsorption.

The initial concentration of dyes is another critical factor effective in the adsorption process (Fig. 8). In this regard, the adsorption behavior was studied at different initial concentrations (100–300 mg L<sup>-1</sup>) for both dyes. According to the  $R_e$

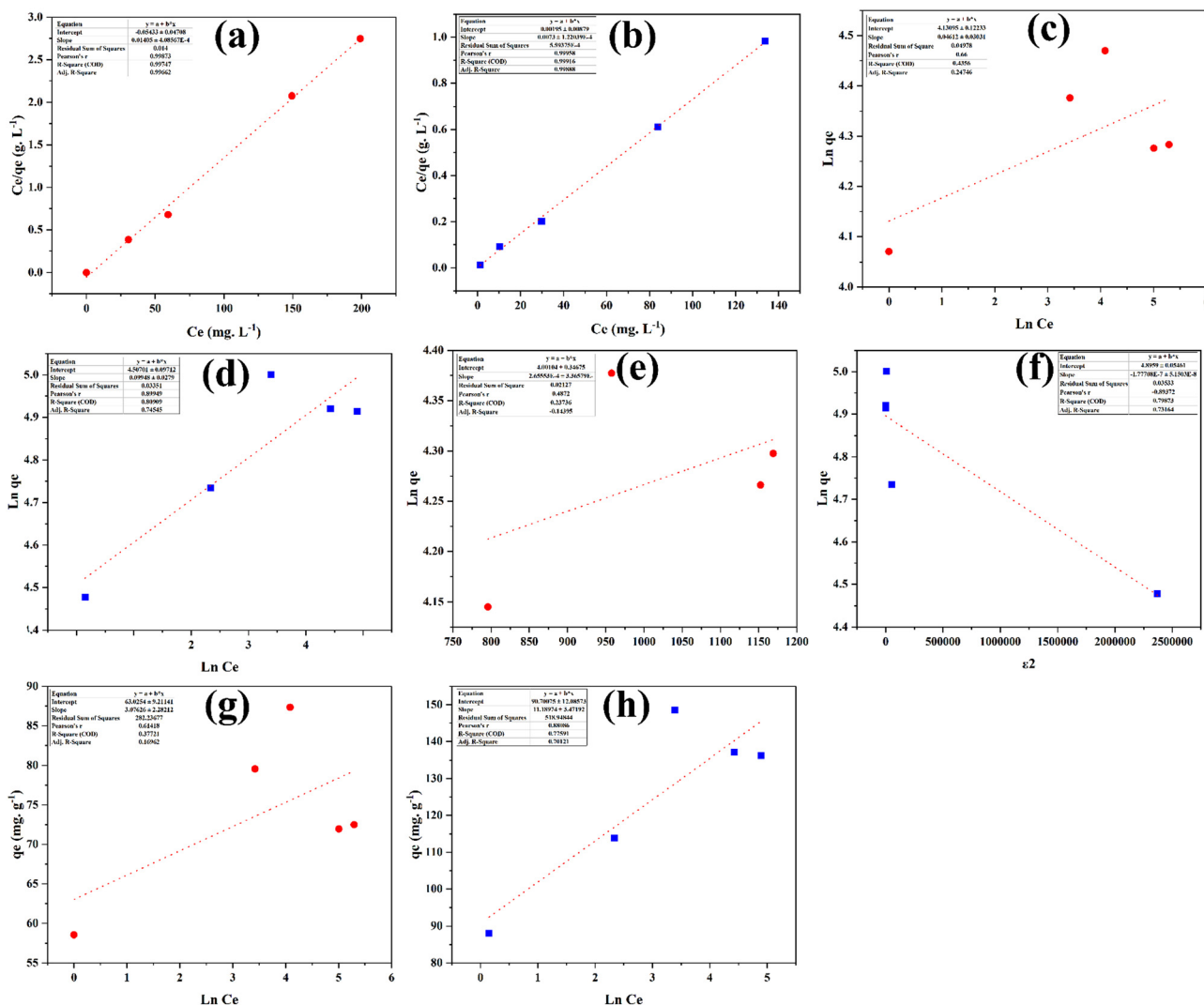


Fig. 10 The isotherm models for Scarlet: (a) Langmuir, (c) Freundlich, (e), Dubinin–Radushkevich, and (g) Temkin; for Congo red: (b) Langmuir, (d) Freundlich, (f), Dubinin–Radushkevich, and (h) Temkin.

Table 2 Isotherm coefficients for the adsorption processes

Model	Langmuir			Freundlich			Temkin			Dubinin–Radushkevich		
	$q_{\max}$	$K_L$	$R^2$	$K_F$	$n$	$R^2$	$A$	$B$	$R^2$	$q_d$	$B$	$R^2$
Adsorbate												
Congo red	71.43	0.26	0.99	13517.6	21.69	0.43	3312.8	3.08	0.38	57.83	$2 \times 10^{-4}$	0.66
Scarlet	136.97	3.84	0.99	32136.6	10.05	0.81	789.8	11.19	0.77	133.74	$-2 \times 10^{-7}$	0.80

values, the initial concentration of  $100 \text{ mg L}^{-1}$  was selected as the optimal concentration for the adsorption of both dyes. The substantial decrease in the  $R_e$  with the increase in the initial concentration could be attributed to the limitation of mass transfer and active-site occupation at higher concentrations.

The amount of adsorbent used to remove Congo red and Scarlet is another influential factor that should be considered.  $R_e$  increases as the adsorbent dosage increases from 2 mg to 6

mg (for 5 mL solution), and a further increase in the adsorbent dosage does not affect  $R_e$ ; therefore, an amount of 6 mg is selected as the optimum amount of adsorbent (Fig. 9).

**3.2.1. Adsorption isotherm.** After optimizing the conditions of the adsorption process, the Langmuir, Freundlich, Dubinin–Radushkevich, and Temkin isotherm models were used to investigate the adsorption behavior. Fig. 10 shows the obtained diagrams of the mentioned isotherms. Comparing the

Table 3 Kinetic coefficients for the adsorption processes

Model	Pseudo-first-order			Pseudo-second-order			Intra-particle diffusion			Elovich			
	Adsorbates	$q_e$	$K_1$	$R^2$	Adsorbates	$q_e$	$K_2$	$R^2$	$K_{id}$	$I$	$R^2$	$\alpha$	$\beta$
Congo red	2.58	0.004	0.91	61.73	238.53	0.99	0.71	50.36	0.91	$5.2 \times 10^6$	2.76	0.97	
Scarlet	9.61	0.0986	0.74	84.03	108.43	0.99	0.28	66.22	0.89	0.225	5.35	0.97	

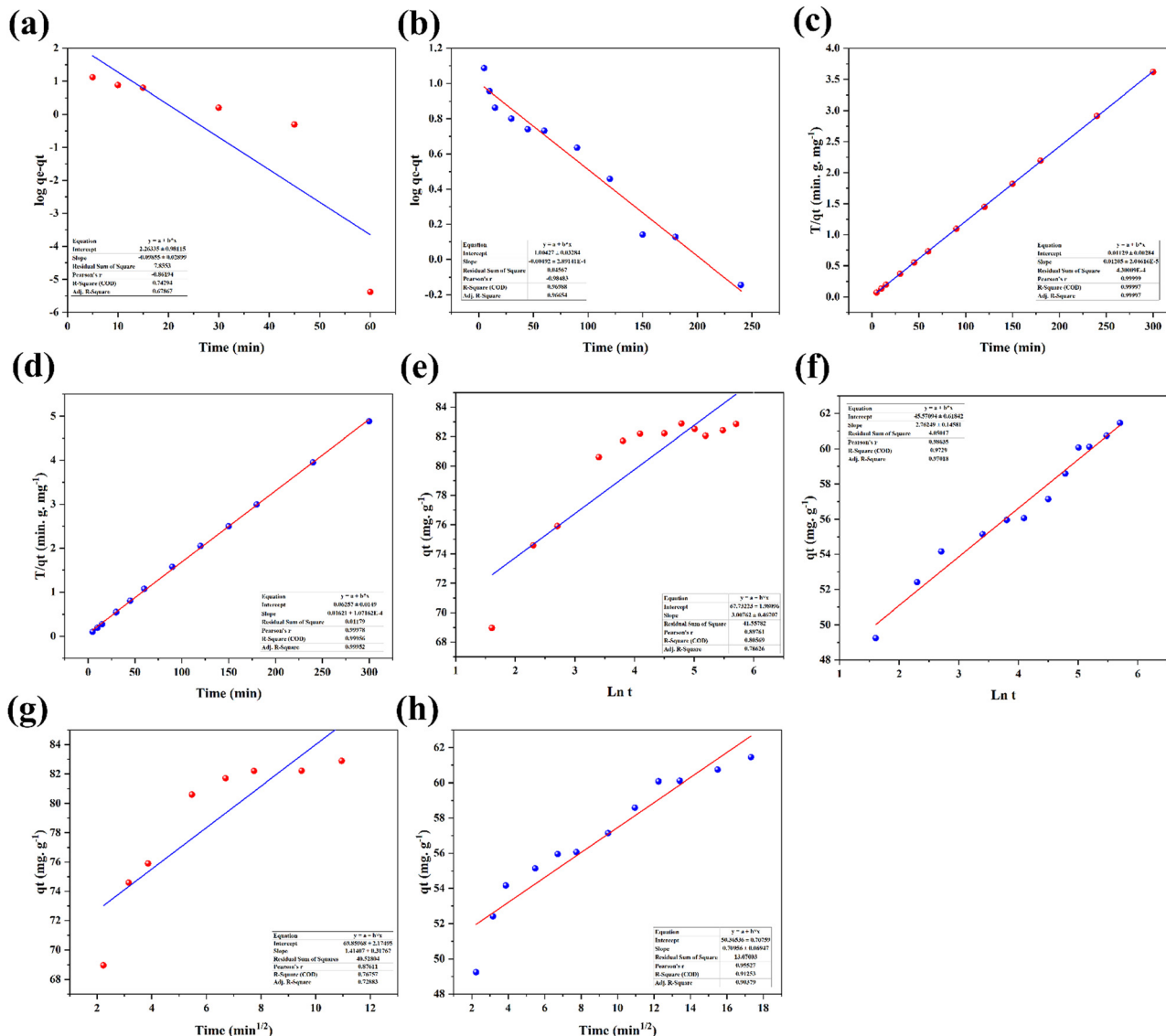


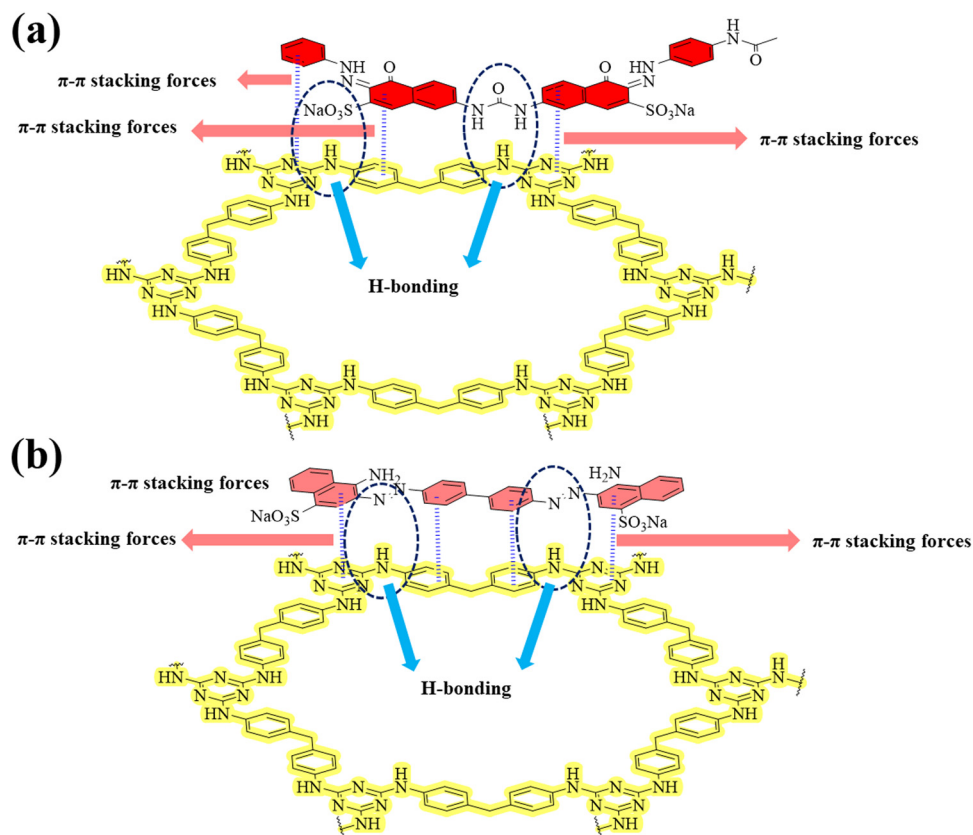
Fig. 11 The kinetic models for Scarlet: (a) Pseudo-first-order, (c) pseudo-second-order, (e), Elovich, and (g) IPD; for Congo red: (b) Pseudo-first-order, (d) Pseudo-second-order, (f), Elovich, and (h) IPD.

correlation coefficient ( $R^2$ ) of these diagrams (Table 2) shows that the adsorption of both dyes obeys the form of Langmuir isotherms and other models failed to describe the adsorption behavior.<sup>51,52</sup> These results indicate that the type of adsorption is monolayer adsorption.

**3.2.2. Adsorption kinetics.** The adsorption kinetics provide excellent information on the rate and the type of interactions in any adsorption process. According to Table 3 and Fig. 11, both dyes obey the pseudo-second-order model proving that the chemical interaction between the adsorbates and adsorbent plays the main role in the rate-determining step. Both dyes are best fitted to the pseudo-second-order model, meaning that the adsorption occurs *via* chemical interactions rather than physical interactions. In the case of Congo red, the adsorption reached the equilibrium within only 150 min, while for the Scarlet the adsorption reached the equilibrium after 60 min. In addition to the pseudo-first-order and pseudo-second-order

models,<sup>52,53</sup> the Elovich and IPD models were also used. The IPD and Elovich models are employed to get a better understanding of the sorption energies.<sup>54</sup> Fig. 11 represents all the kinetic diagrams of the adsorption of Congo red and Scarlet dyes.<sup>55</sup> The IPD model shows the four steps of adsorption: (i) diffusion of dye molecules from solution to the outer surface of the adsorbent, (ii) adsorption of dye molecules on the outer surface of the adsorbent, (iii) diffusion of dye molecules into the interior surface of the adsorbent, and (iv) adsorption of dye molecules on the active centers present in the interior surface of the adsorbent. By comparing the regression of IPD of Congo red and Scarlet adsorption, it was observed that Congo red fits better to the IPD model than Scarlet. Also, a similar comparison of the regression coefficient using the Elovich model shows that the adsorption processes for both dyes have a chemisorption nature.<sup>46,47,56,57</sup>

**3.2.3. Adsorption mechanism.** Generally, different types of mechanisms are involved in the adsorption processes, including



Scheme 2 Schematic illustration of interactions in the adsorption process for (a) Scarlet and (b) Congo red.

Table 4 Thermodynamic data for the adsorption processes

Parameters	$\Delta S^\circ$ (kJ mol <sup>-1</sup> K <sup>-1</sup> )	$\Delta H^\circ$ (kJ mol <sup>-1</sup> )	$\Delta G^\circ$ (kJ mol <sup>-1</sup> )				
			Temperature (K)	288	298	308	318
Congo red	0.651	-178.825		-366.313	-372.823	-379.333	-385.843
Scarlet	0.280	-75.386		-156.026	-158.826	-161.626	-164.426

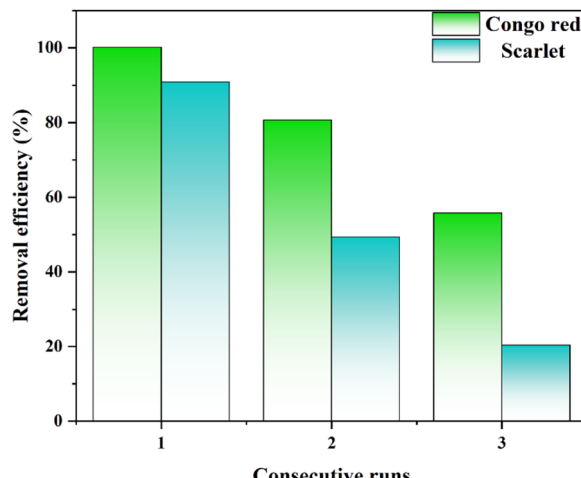


Fig. 12 The reusability of the MDA-POP after three successive cycles.

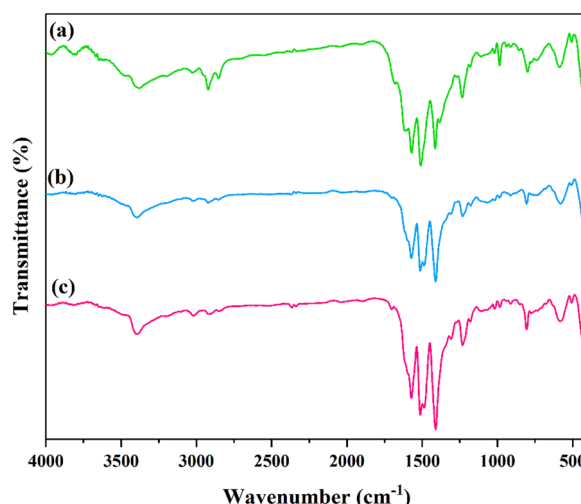


Fig. 13 FTIR spectra of (a) pristine MDA-POP, (b) after 3 consecutive adsorption/desorption cycles of Congo red, and (c) after 3 consecutive adsorption/desorption cycles of Scarlet.

van der Waals forces, aggregation mechanisms, physical adsorption, hydrophobic attractions, hydrogen bonding, electrostatic interactions, and chemical bonding.<sup>58</sup> Since the adsorption kinetics was best fitted to the pseudo-second-order model and

its excellent tendency to the Elovich model, hydrogen bonding and  $\pi-\pi$  interactions dominate the adsorption process (Scheme 2). The presence of aromatic rings in the dye structures strongly supports the idea of the existence of  $\pi-\pi$  stacking forces in the adsorption process. More importantly, the amine-rich structure of the MDA-POP caused the formation of H-bonding interactions during adsorption.

**3.2.4. Adsorption thermodynamics.** The thermodynamic values provide deeper insights into intrinsic energy changes during adsorption. According to the van't Hoff equation, the standard Gibbs free energy ( $\Delta G^\circ$ ) indicates whether a process is spontaneous or not. Table 4 summarizes the thermodynamic values obtained at four different temperatures. The negative value of  $\Delta G^\circ$  for the adsorption of Scarlet indicates it is a spontaneous process. The negative values for  $\Delta H^\circ$  indicate that the dye removal is a chemisorption process. However, the adsorption of Congo red is negligibly affected by the increase in temperature, which means that the adsorption of Congo red does not change as a function of temperature.

### 3.4. Reusability test

To study the reusability and recyclability of the MDA-POP, the adsorbent was washed with methanol, acetone, and ethanol and dried to use it for the next cycle. It was found that methanol is the best eluent for the desorption of Scarlet and ethanol is the best for Congo red desorption. Since the chemical interactions play the main role in the adsorption process, the removal efficiency decreased after each cycle (Fig. 12). The FTIR spectra of the MDA-POP after using three times show a nearly identical form proving the structural stability of the MDA-POP (Fig. 13).

### 3.5. Comparison of the efficiency of the MDA-POP with that of reported adsorbents

Different types of materials have been used in removing dyes from water and wastewater; however, finding new adsorbents is of paramount interest. Table 5 summarizes recent studies on removing Congo red and Scarlet from wastewater, using natural materials (entry 1), nanocomposites (entries 2 and 3), COFs (entry 4), polymers (entry 5), and graphene oxide (entries 6 and 7). Although the performance of the MDA-POP was lower than that of the benchmark adsorbents like TCOF (Table 5, entry 4), the more facile synthesis procedure and satisfactory results compared to the traditionally used materials such as polymers

Table 5 A comparison of the MDA-POP with recent adsorbents for dye removal

Entry	Adsorbents	Adsorbates	$C_i$ (mg L <sup>-1</sup> )	Time (min)	$q_e$ (mg L <sup>-1</sup> )	Ref.
1	Natural down fibers	Scarlet	500	150	120.34	59
2	PANI/ZTO	Congo red	50	15	64.51	60
3	FC-POP -EDA@Fe <sub>3</sub> O <sub>4</sub>	Scarlet	300	240	32.13	61
4	N-rich TCOF	Scarlet	1000	360	8501	62
5	Polyaniline	Congo red	20	30	50	63
6	PVA-PAA-GO-COOH-PDA	Congo red	25	240	9.62	64
7	pTSA@PANI@GO	Congo red	200	150	66.66	65
8	<b>MDA-POP</b>	<b>Scarlet</b>	<b>100</b>	<b>60</b>	<b>137</b>	<b>Present study</b>
		<b>Congo red</b>	<b>100</b>	<b>150</b>	<b>72</b>	

and nanocomposites, make MDA-POP a great candidate to be prepared on large scales and used in water remediation.

## 4. Conclusions

In conclusion, an amine-rich porous organic polymer with excellent flexibility was synthesized from 2,4,6-trichloro-1,3,5-triazine (TCT) and 4,4'-methylenedianiline (MDA) using a facile method. The prepared MDA-POP was used in removing Congo red and Scarlet 4BS from aqueous solutions. The MDA-POP shows a maximum adsorption capacity of  $71.43 \text{ mg g}^{-1}$  for Congo red and  $136.97 \text{ mg g}^{-1}$  for Scarlet 4BS. Different adsorption isotherms were investigated, and the obtained data were best fitted to the Langmuir model representing monolayer adsorption. Also, the pseudo-second-order model is found to be the best model for describing the adsorption process, which indicates that the nature of the adsorption is chemisorption. The thermodynamic studies show a spontaneous adsorption process. This paper provides a facile and efficient method for synthesising POPs as adsorbents for water treatment applications.

## Conflicts of interest

There are no conflicts of interest to declare.

## Acknowledgements

The authors wish to thank the research council of the Isfahan University of Technology.

## References

- N. Mokhtari, M. Afshari and M. Dinari, *Polymer*, 2020, **195**, 122430.
- T. Islam, M. R. Repon, T. Islam, Z. Sarwar and M. M. Rahman, *Environ. Sci. Pollut. Res.*, 2023, **30**, 9207–9242.
- C. A. Martínez-Huitl, M. A. Rodrigo, I. Sirés and O. Scialdone, *Chem. Rev.*, 2015, **115**, 13362–13407.
- C.-C. Wang, J.-R. Li, X.-L. Lv, Y.-Q. Zhang and G. Guo, *Energy Environ. Sci.*, 2014, **7**, 2831–2867.
- B. C. Ma, S. Ghasimi, K. Landfester, F. Vilela and K. A. Zhang, *J. Mater. Chem. A*, 2015, **3**, 16064–16071.
- B. Wang, Z. Xie, Y. Li, Z. Yang and L. Chen, *Macromolecules*, 2018, **51**, 3443–3449.
- Y. Liu, Y. Wang, H. Li, X. Guan, L. Zhu, M. Xue, Y. Yan, V. Valtchev, S. Qiu and Q. Fang, *Chem. Sci.*, 2019, **10**, 10815–10820.
- I. Ali, *Chem. Rev.*, 2012, **112**, 5073–5091.
- B. Chen, Q. Ma, C. Tan, T. T. Lim, L. Huang and H. Zhang, *Small*, 2015, **11**, 3319–3336.
- B. Boukoussa, A. Mokhtar, A. El Guerdaoui, M. Hachemaoui, H. Ouachtak, S. Abdelkrim, A. A. Addi, S. Babou, B. Boudina and A. Bengueddach, *J. Mol. Liq.*, 2021, **333**, 115976.
- X. Xie, X. Huang, W. Lin, Y. Chen, X. Lang, Y. Wang, L. Gao, H. Zhu and J. Chen, *ACS Omega*, 2020, **5**, 13595–13600.
- A. Tchinsa, M. F. Hossain, T. Wang and Y. Zhou, *Chemosphere*, 2021, **284**, 131393.
- W. Schwieger, A. G. Machoke, T. Weissenberger, A. Inayat, T. Selvam, M. Klumpp and A. Inayat, *Chem. Soc. Rev.*, 2016, **45**, 3353–3376.
- H. F. Youssef, R. A. Nasr, E. A. Abou El-Anwar, H. S. Mekky and S. H. Abd El Rahim, *Microporous Mesoporous Mater.*, 2021, **328**, 111485.
- Y. Li, X. Yan, X. Hu, R. Feng and M. Zhou, *Chem. Eng. J.*, 2019, **375**, 122003.
- S. Moosavi, C. W. Lai, S. Gan, G. Zamiri, O. Akbarzadeh Pivezhani and M. R. Johan, *ACS Omega*, 2020, **5**, 20684–20697.
- C. Patawat, K. Silakate, S. Chuan-Udom, N. Supanchaiyamat, A. J. Hunt and Y. Ngernyen, *RSC Adv.*, 2020, **10**, 21082–21091.
- N. Theamwong, W. Intarabumrung, S. Sangon, S. Aintharabunya, Y. Ngernyen, A. J. Hunt and N. Supanchaiyamat, *Bioresour. Technol.*, 2021, **341**, 125832.
- Y. Hou, X. Zhang, C. Wang, D. Qi, Y. Gu, Z. Wang and J. Jiang, *New J. Chem.*, 2017, **41**, 6145–6151.
- Y. Yuan, H. Huang, L. Chen and Y. Chen, *Macromolecules*, 2017, **50**, 4993–5003.
- N. Taheri, M. Dinari and M. Asgar, *ACS Appl. Polym. Mater.*, 2022, **4**, 6288–6302.
- M. Ding, X. Cai and H.-L. Jiang, *Chem. Sci.*, 2019, **10**, 10209–10230.
- X. Shen, S. Ma, H. Xia, Z. Shi, Y. Mu and X. Liu, *J. Mater. Chem. A*, 2018, **6**, 20653–20658.
- Y. Shen, W.-X. Ni and B. Li, *ACS Omega*, 2021, **6**, 3202–3208.
- L. Chen, K. Furukawa, J. Gao, A. Nagai, T. Nakamura, Y. Dong and D. Jiang, *J. Am. Chem. Soc.*, 2014, **136**, 9806–9809.
- S. Wan, J. Guo, J. Kim, H. Ihee and D. Jiang, *Angew. Chem., Int. Ed.*, 2009, **48**, 5439–5442.
- Q. Chen, M. Luo, P. Hammershøj, D. Zhou, Y. Han, B. W. Laursen, C.-G. Yan and B.-H. Han, *J. Am. Chem. Soc.*, 2012, **134**, 6084–6087.
- C. Lu, T. Ben and S. Qiu, *Macromol. Chem. Phys.*, 2016, **217**, 1995–2003.
- Y.-Q. Shi, J. Zhu, X.-Q. Liu, J.-C. Geng and L.-B. Sun, *ACS Appl. Mater. Interfaces*, 2014, **6**, 20340–20349.
- Y.-C. Zhao, T. Wang, L.-M. Zhang, Y. Cui and B.-H. Han, *ACS Appl. Mater. Interfaces*, 2012, **4**, 6975–6981.
- W.-C. Song, X.-K. Xu, Q. Chen, Z.-Z. Zhuang and X.-H. Bu, *Polym. Chem.*, 2013, **4**, 4690–4696.
- R. Ullah, M. Atilhan, B. Anaya, S. Al-Muhtaseb, S. Aparicio, H. Patel, D. Thirion and C. T. Yavuz, *ACS Appl. Mater. Interfaces*, 2016, **8**, 20772–20785.
- N. Mokhtari, M. Dinari and O. Rahamanian, *Polym. Int.*, 2019, **68**, 1178–1185.
- D. He, L. Jiang, K. Yuan, J. Zhang, J. Zhang, Q. Fan, H. Liu and S. Song, *Chem. Eng. J.*, 2022, **446**, 137119.
- N. A. Babujohn, P. Shifana, A. Eluri and K. Thahaliya, *Sep. Purif. Technol.*, 2023, **316**, 123770.

- 36 F. Rezaei and M. Dinari, *Microporous Mesoporous Mater.*, 2021, **325**, 111339.
- 37 J. Mondal, Q. T. Trinh, A. Jana, W. K. H. Ng, P. Borah, H. Hirao and Y. Zhao, *ACS Appl. Mater. Interfaces*, 2016, **8**, 15307–15319.
- 38 R. K. Totten, Y.-S. Kim, M. H. Weston, O. K. Farha, J. T. Hupp and S. T. Nguyen, *J. Am. Chem. Soc.*, 2013, **135**, 11720–11723.
- 39 W. Wang, C. Li, L. Yan, Y. Wang, M. Jiang and Y. Ding, *ACS Catal.*, 2016, **6**, 6091–6100.
- 40 Y. Sang, Y. Cao, L. Wang, W. Yan, T. Chen, J. Huang and Y.-N. Liu, *J. Colloid Interface Sci.*, 2021, **587**, 121–130.
- 41 M. Afshari, M. Dinari, H. Moradi and Z. Noori, *Polym. Adv. Technol.*, 2020, **31**, 2433–2442.
- 42 I. X. García-Zubiri, G. González-Gaitano and J. R. Isasi, *J. Colloid Interface Sci.*, 2009, **337**, 11–18.
- 43 M. Doğan, Y. Özdemir and M. Alkan, *Dyes Pigm.*, 2007, **75**, 701–713.
- 44 D. Mahanta, G. Madras, S. Radhakrishnan and S. Patil, *J. Phys. Chem. B*, 2008, **112**, 10153–10157.
- 45 L. Wang and A. Wang, *J. Hazard. Mater.*, 2007, **147**, 979–985.
- 46 C. Păcurariu, O. Paşka, R. Ianoş and S. G. Muntean, *Clean Technol. Environ. Policy*, 2016, **18**, 705–715.
- 47 S. G. Muntean, M. E. Rădulescu-Grad and P. Sfărloagă, *RSC Adv.*, 2014, **4**, 27354–27362.
- 48 G. Xiong, B.-B. Wang, L.-X. You, B.-Y. Ren, Y.-K. He, F. Ding, I. Dragutan, V. Dragutan and Y.-G. Sun, *J. Mater. Chem. A*, 2019, **7**, 393–404.
- 49 L. Tian, S. Zhou, J. Zhao, Q. Xu, N. Li, D. Chen, H. Li, J. He and J. Lu, *J. Hazard. Mater.*, 2022, 129873.
- 50 B. Wang, Q. Zhang, G. Xiong, F. Ding, Y. He, B. Ren, L. You, X. Fan, C. Hardacre and Y. Sun, *Chem. Eng. J.*, 2019, **366**, 404–414.
- 51 G. Zhou, J. Luo, C. Liu, L. Chu and J. Crittenden, *Water Res.*, 2018, **131**, 246–254.
- 52 W. Zhang, S. Zhang, J. Wang, M. Wang, Q. He, J. Song, H. Wang and J. Zhou, *Chemosphere*, 2018, **203**, 188–198.
- 53 S. Chen, J. Wang, Z. Wu, Q. Deng, W. Tu, G. Dai, Z. Zeng and S. Deng, *J. Colloid Interface Sci.*, 2018, **523**, 110–120.
- 54 S. Shi, J. Yang, S. Liang, M. Li, Q. Gan, K. Xiao and J. Hu, *Sci. Total Environ.*, 2018, **628**, 499–508.
- 55 V. Manirethan, K. Raval, R. Rajan, H. Thaira and R. M. Balakrishnan, *J. Environ. Manage.*, 2018, **214**, 315–324.
- 56 S. G. Muntean, A. Todea, M. E. Rădulescu-Grad and A. Popa, *Pure Appl. Chem.*, 2014, **86**, 1771–1780.
- 57 S. G. Muntean, O. Paska, S. Coseri, G. M. Simu, M. E. Grad and G. Ilia, *J. Appl. Polym. Sci.*, 2013, **127**, 4409–4421.
- 58 C. Shen, Y. Shen, Y. Wen, H. Wang and W. Liu, *Water Res.*, 2011, **45**, 5200–5210.
- 59 F. Chen, L. Xiong, M. Cai, W. Xu and X. Liu, *Fibers Polym.*, 2015, **16**, 73–78.
- 60 S. Singh, S. Perween and A. Ranjan, *J. Environ. Chem. Eng.*, 2021, **9**, 105149.
- 61 N. Taheri and M. Dinari, *New J. Chem.*, 2022, **46**, 11174–11184.
- 62 M. Afshari and M. Dinari, *J. Hazard. Mater.*, 2020, **385**, 121514.
- 63 H. Chafai, M. Laabd, S. Elbariji, M. Bazzaoui and A. Albourine, *J. Dispersion Sci. Technol.*, 2017, **38**, 832–836.
- 64 R. Xing, W. Wang, T. Jiao, K. Ma, Q. Zhang, W. Hong, H. Qiu, J. Zhou, L. Zhang and Q. Peng, *ACS Sustainable Chem. Eng.*, 2017, **5**, 4948–4956.
- 65 M. O. Ansari, R. Kumar, S. A. Ansari, S. P. Ansari, M. Barakat, A. Alshahri and M. H. Cho, *J. Colloid Interface Sci.*, 2017, **496**, 407–415.